# Modeling and Simulation of Infrared Signature of Remote Aerial Targets

Bendong Zhao, Shanzhu Xiao, Huanzhang Lu, and Dongya Wu
Automatic Target Recognition Laboratory
National University of Defense Technology
Changsha, China

***Abstract*—A modeling and simulation method of infrared signature of remote aerial targets is presented in this paper. It takes a comprehensive consideration of the influence of shape, material, attitude, motion and surface temperature field of the target. Firstly, the geometric shape of targets are modeled. Then motion models are built to obtain the position and attitude of targets in real time. Next, we divide the target surface into hundreds of grids and calculate its temperature distribution by establishing a thermal equilibrium equation for each grid. Finally, the infrared radiation power received by the detector from the target can be achieved according to above analyses and the observation condition. Simulation results demonstrate that targets with different shape or different motion information have different infrared radiation characteristics, which provides a feasibility of using infrared signature for remote aerial targets recognition.**

***Keywords—modeling and simulation; infrared signature; remote aerial targets***

## I. INTRODUCTION

With the rapid development of space technology, a great increasing number of aerial objects such as satellites and ballistic targets are launched into the outer space. Detection and recognition of these targets is an important topic in many areas. For example, in aerospace science, it can help cataloging and managing the hundreds of satellites. And in military field, it can be used to help detecting and recognizing the warring targets. Therefore, it has attracted great interest and tremendous effort during last decades. However, it still remains a challenging problem as the targets are always very far away from us and difficult for observation.

Because of high sensitivity, strong anti-interference ability and no limit for service time, infrared (IR) imaging technique is rapidly developed and widely used in many areas such as IR searching and tracking system and remote sensing. In recent years, a great amount of researches on infrared targets detection and recognition can be found in literatures [1-6]. Generally, a lot of test data are always needed to verify the detection and recognition performance of the proposed method while studying a novel algorithm. However, data acquisition is always a hard problem due to the following three factors: 1) time consuming and spending expensive, especially for the remote aerial targets, 2) difficult to obtain enough data of different targets, motion models and observation conditions and 3) data of some military targets are more difficult to obtain. To overcome this limitation, many scholars have done a great deal of researches on modeling and simulation of infrared signature of targets [7-9]. According to the geometrical optics and radiation theory, the infrared characteristics of remote aerial targets depend on the geometric shape, material, attitude, surface temperature distribution of the target and the observation condition. This paper takes a comprehensive consideration of these factors to model and simulate the infrared signature of remote aerial targets. The remaining part of this paper is organized as follows. In Section II, the modeling and simulation methods are described in detail. Experiments and discussions are shown in Section III and conclusion follows in Section IV.

## II. Approaches

### A. Geometric shape models

The most common shapes of aerial targets include sphere, cubic, cylinder, cone and their combination body. In order to represent the difference, three basic shape models of sphere, cylinder and cone are chosen as our geometric models in this paper. Electromagnetic simulation software FEKO is used for shape modeling and facet division, as shown in Fig. 1.

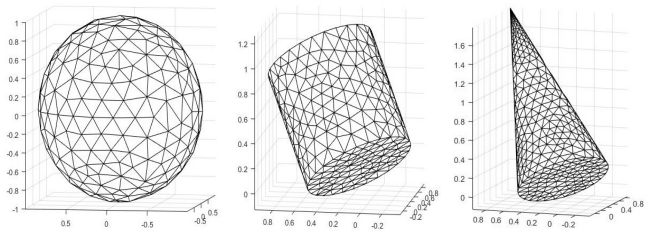

(a) Sphere (b) Cylinder (c) Cone

Fig. 1. Three basic shape models of targets

### B. Motion models

The purpose of motion modeling is to obtain the position and attitude of targets in real time. It is composed of two

978-1-5386-1937-7/17/$31.00 ©2017 IEEE

parts: trajectory modeling and attitude modeling. Trajectory modeling is used to obtain the target position in real time and attitude modeling is used to obtain the target attitude. The two models are discussed individually in detail in this section.

(1) Trajectory modeling

The midcourse ballistic targets are considered as our major objects in this paper. Therefore, ballistic trajectories are need to be modeled firstly. Here we make the following three assumptions :1) The influence of the moon and other stars is ignored because the targets are very close to the earth during flight; 2) The influence of atmosphere is also ignored because the midcourse ballistic targets fly outside of the atmosphere; and 3) The earth is regarded as a uniform sphere and the influence of its revolution and rotation is ignored.

Based on above assumptions, the ballistic trajectory is an elliptic orbit, as shown in Fig. 2. Curve $BC$ represents the trajectory, $V$ is the target velocity which can be decomposed into radial velocity $V_r$ and circumferential velocity $V_f$, $\theta$ is the angle between $V$ and $V_f$. $O_e$ represents the center of the earth, and $r$ denotes the distance between the target and $O_e$. $F$ and $f$ denote the eccentric anomaly and the true anomaly respectively.

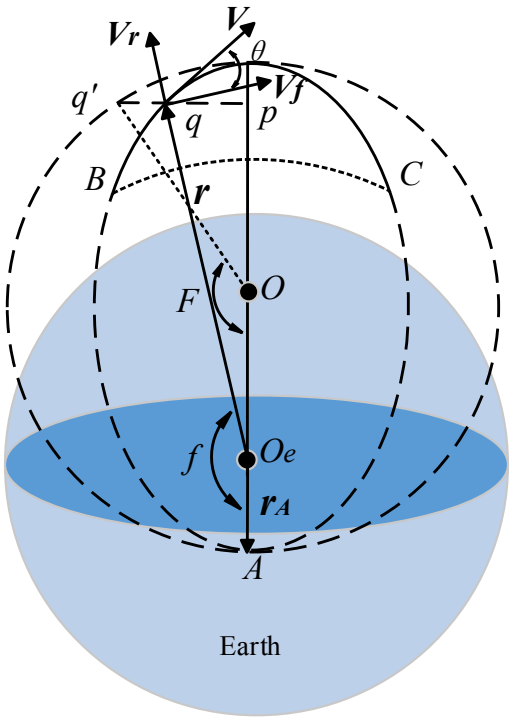


Fig. 2. The ballistic trajectories solution

According to the ballistic theory, the only elliptic orbit can be obtained if the initial parameters $r_0$, $V_0$ and $\theta_0$ of the target are determined. Moreover, the parameters $r_t$, $V_t$ and $\theta_t$ of the target at any time can be computed according to the following four steps:

Step 1: According to the law of conservation of moment of momentum and the law of conservation of mechanical energy, the elliptic orbit can be solved, and the parameters of elliptic orbit can be obtained according to $r_0$, $V_0$ and $\theta_0$, as shown in Eq. (1).

$$\begin{aligned} e &= \sqrt{1+\gamma_0(\gamma_0-2)\cos^2\theta_0} \\ a &= \frac{\mu r_0}{2\mu - V_0^2 r_0} \\ b &= \sqrt{\frac{\gamma_0}{2-\gamma_0}} r_0 \cos\theta_0 \end{aligned} \tag{1}$$

where $e$ denotes the eccentricity of the orbit, $\gamma_0 = \frac{V_0^2}{\mu / r_0}$ is an energy parameter, $\mu = GM = 3.99\times10^{14}\ \mathrm{m^3/s^2}$ is the gravitational constant, $a$ and $b$ denote the semi-major and semi-minor axis of the orbit respectively.

Step 2: Compute the initial eccentric anomaly $F_0$ according to the elliptic parameters $e$, $a$, and the initial distance $r_0$, as described in Eq. (2).

$$F_0 = \arccos\frac{1-r_0/a}{e} \tag{2}$$

Step 3: According to the Kepler's second law, we can establish the Kepler equation, as shown in Eq. (3), in which $\omega$ denotes the average angular velocity of the target, and it can be represented as $\omega = \sqrt{\mu/a^3}$ according to the Kapler's third law.

$$M = \omega(t - t_A) = F - e\sin F \tag{3}$$

where $t_A$ denotes the time when the target reaches the perigee and it can be computed according to $F_0$, then the eccentric anomaly at any time $F_t$ can be computed according to Eq. (3).

Step 4: Compute the target parameters $r_t$, $V_t$ and $\theta_t$ at any time according to $F_t$ , as described in Eq. (4).

$$\begin{aligned} r_t &= a(1-e\cos F_t) \\ V_t &= \sqrt{\mu/a}\,\frac{\sqrt{1-e^2\cos^2 F_t}}{1-e\cos F_t} \\ \theta_t &= \arctan\frac{e\sin F_t}{\sqrt{1-e^2}} \end{aligned} \tag{4}$$

(2) Attitude modeling

Micro-motion of the midcourse ballistic targets is the main reason for attitude change. Two micro-motion models of rotation and precession are considered in this paper, as shown in Fig. 3, which are briefly described respectively below.

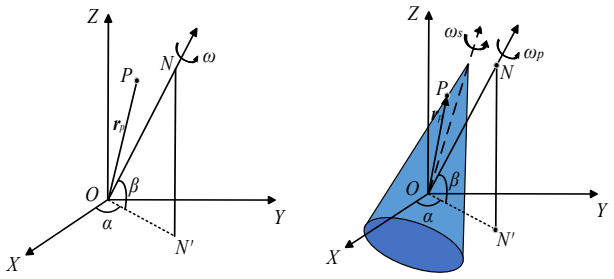


(a) Rotation (b) Precession

Fig. 3. Two micro-motion models

As shown in Fig. 3 (a), *ON* is the rotation axis, $\alpha$ and $\beta$ denote its azimuth and pitch angle respectively, so its unit vector can be written as $\boldsymbol{e}=[\cos\beta\cos\alpha,\cos\beta\sin\alpha,\sin\beta]^T$. The rotation angle velocity is set as $\omega$, assumes the initial position of point *P* is $\boldsymbol{r}_p=(x_p,y_p,z_p)^T$, then the position of point *P* at time *t* can be written as $\boldsymbol{r}_p(t)=\boldsymbol{T}\boldsymbol{r}_p$. Where rotation matrix is

$$\boldsymbol{T}=\boldsymbol{I}+\hat{\boldsymbol{e}}\sin\omega t+\hat{\boldsymbol{e}}^2(1-\cos\omega t) \tag{5}$$

where $\boldsymbol{I}$ is an identity matrix, and $\hat{\boldsymbol{e}}$ is the cross product matrix of $\boldsymbol{e}$, i.e., $\boldsymbol{e}\times\boldsymbol{r}_p=\hat{\boldsymbol{e}}\cdot\boldsymbol{r}_p$, which can be expressed as Eq. (6).

$$\hat{\boldsymbol{e}}=\begin{bmatrix}0 & -\sin\beta & \sin\alpha\cos\beta\\ \sin\beta & 0 & -\cos\alpha\cos\beta\\ -\sin\alpha\cos\beta & \cos\alpha\cos\beta & 0\end{bmatrix} \tag{6}$$

The precession can be seen as a superposition of two rotations, as shown in Fig. 3 (b). The target rotates around its symmetry axis with an angle velocity $\omega_s$, and the symmetry axis rotates around the precession axis *ON* with an angle velocity $\omega_p$, *ON* intersects with the symmetry axis at the ordinate origin. Assumes the initial position of point *P* is $\boldsymbol{r}_p=(x_p,y_p,z_p)^T$, then the position of point *P* at time *t* can be written as $\boldsymbol{r}_p(t)=\boldsymbol{T}_p\boldsymbol{T}_s\boldsymbol{r}_p$. Where rotation matrix $\boldsymbol{T}_p$ and $\boldsymbol{T}_s$ can be obtained using the same method as described in Eq. (5).

### C. Surface temperature distribution

The temperature distribution of the target surface can be calculated by using node network method and the thermal equilibrium equation for grid *i* can be written as

$$Q_1+Q_2+Q_3+Q_4+Q_5+Q_6-Q_7=c\rho A_i d_i\frac{dT_i}{dt}\ . \tag{7}$$

where $Q_1\sim Q_6$ represent the infrared radiation absorbed by the grid, $Q_7$ is the radiation emitted by the grid, $c$ and $\rho$ denote specific heat ratio and density of the material respectively, $A_i$, $d_i$ and $T_i$ are surface area, thickness and surface temperature of the grid respectively, and $t$ is time. Next, we will give a brief description about $Q_1\sim Q_7$.

$Q_1$ is direct solar radiation absorbed by the grid, which can be expressed as Eq. (8), where $\varepsilon$ is emissivity of the material, $S_0=1366\ \mathrm{W/m^2}$ is the solar constant, and $F_{Si}$ is radiation angle factor. $Q_2$ is emitted infrared radiation of the earth absorbed by the grid, which can be expressed as Eq. (9), where $\rho_0=0.35$ denotes the average reflectivity of the earth. $Q_3$ is reflected infrared radiation of the earth absorbed by the grid, which can be expressed as Eq. (10). $Q_4$ is radiation absorbed by the grid from the internal heat source $K$ of the target, which can be expressed as Eq. (11). $Q_5$ is the heat transferred from the adjacent grids, which can be expressed as Eq. (12), where $j$ is the adjacent grid, $A_{ij}$ is the contact area between grid $i$ and $j$, $L_{ij}$ is the distance between grid $i$ and $j$, $k$ denotes heat conductivity. $Q_6$ is infrared radiation absorbed by the grid from other grids, as we consider targets convex bodies in this paper, so $Q_6=0$. $Q_7$ is the radiation emitted by the grid, which can be expressed as Eq. (13) according to Stefan Boltzmann's law, where $\sigma=5.6697\times10^{-8}\ \mathrm{W/(m^2\cdot K^4)}$ is Stefan Boltzmann constant.

$$Q_1=\varepsilon S_0 A_i F_{Si} \tag{8}$$

$$Q_2=\varepsilon(1-\rho_0)S_0 A_i F_{Ei}/4 \tag{9}$$

$$Q_3=\varepsilon\rho_0 S_0 A_i F_{SEi} \tag{10}$$

$$Q_4=K\cdot A_i\Big/\sum\nolimits_i A_i \tag{11}$$

$$Q_5=\sum\nolimits_j k\cdot A_{ij}\cdot(T_j-T_i)/L_{ij} \tag{12}$$

$$Q_7=\varepsilon\sigma T^4 \tag{13}$$

### D. Radiation power calculation

Radiation power calculation is the key step of the IR signature simulation. According to Planck's law of radiation, the spectral radiance of a target with temperature $T$ at wavelength $\lambda$ can be written as

$$M(\lambda,T)=\frac{\varepsilon C_1}{\lambda^5(e^{C_2/\lambda T}-1)}\ . \tag{14}$$

where $\varepsilon$ is emissivity of the material, $C_1=2\pi hc^2$ is the first radiation constant, and $C_2=hc/k$ is the second radiation constant, in which $h=6.63\times10^{-34}\ \mathrm{J\cdot s}$ is Planck constant, $c$ is the speed of light in vacuum, and $k=1.38\times10^{-23}\ \mathrm{J/K}$ is Boltzmann constant.

As shown in Fig. 4, $n_i$ is the normal vector of a facet with area $A_i$, the distance between the facet and the detector is $R$, and $o_i$ is the normal vector of the aperture of the optical system. According to Lambert cosine theorem, the radiant

intensity of the facet along the direction of facet-to-detector can be expressed as

$$I_\alpha = \frac{A_i \int M(\lambda,T)d\lambda}{\pi}\cos\alpha \tag{15}$$

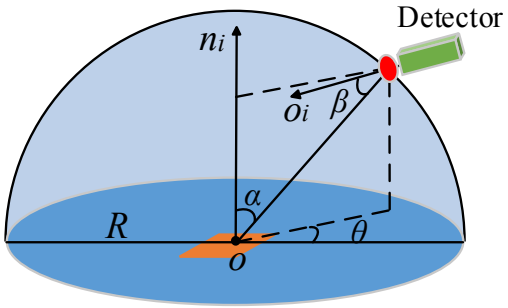


Fig. 4. Diagram of radiation energy reception

Assume the aperture area is $A_0$, then it's effective area of receiving radiation is $A_0\cos\beta$. The solid angle of the detector to the facet is $A_0\cos\beta/R^2$, thus the radiation power of the facet at the aperture in the wavelength range of $\lambda_1$~$\lambda_2$ can be expressed as

$$P = \frac{A_0 A_i F_{Di}\int_{\lambda_1}^{\lambda_2} M(\lambda,T)d\lambda}{\pi R^2} \tag{16}$$

where $F_{Di}$ is radiation angle factor, which can be written as

$$F_{Di} = \begin{cases} \cos\alpha\cdot\cos\beta & \cos\alpha>0 \text{ and } \cos\beta>0 \\ 0 & \text{others} \end{cases}. \tag{17}$$

## III. SIMULATION RESULTS & DISCUSSION

This section validates the models proposed in this paper and three assumptions are made as follows: 1) The IR detector moves towards the target with constant velocity all the time. And the target has always been in the field of view of the detector, changing from dim to bright gradually; 2) The target and detector both fly outside of the atmosphere, so the energy attenuation during transmission is neglected; 3) The target is far away from the IR detector and presents as a single pixel bright point on the imaging plane. So we just need to obtain the time series of targets' IR radiation power rather than sequence images. Three groups of experiments are conducted to verify the influence of target shape, target micro-motion model and micro-motion parameters on the simulation results.

### A. Trajectories of target and detector

Set the initial position and velocity of the target as follows:

$$r_0 = 6471\text{ km}, V_0 = 6\text{ km/s}, \theta_0 = \pi/6\ . \tag{18}$$

Set the initial position of the detector 300 km away from the target, and move towards it at a speed of 4 km/s. Their trajectories in 20 seconds are shown in Fig. 5.

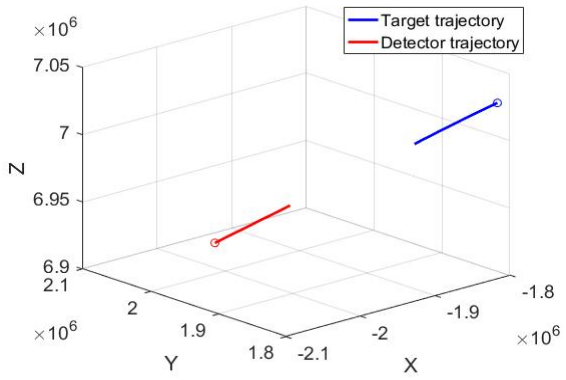


Fig. 5. Trajectories of target and detector in 20 seconds

### B. Values of parameters

There are many parameters of target and detector in our proposed method need to be determined in advance. They are set as shown in Table I.

TABLE I. Parameters setting of target and detector

| Target | | Detector | |
|---|---|---|---|
| Initial temperature | $T$=300 K | Frame frequency | $f$=10 Hz |
| Surface thickness | $d$=2 cm | | |
| Emissivity | $\varepsilon$=0.5 | Optical aperture | $D$=0.5 m |
| Heat conductivity | $k$=0.1 | | |
| Specific heat ratio | $c$=837 J/kg•K | Wavelength range | 3.7~4.8 μm |
| Density | $\rho$=2700 kg/m$^3$ | | |
| Internal heat source | 100 W | | |

### C. Simulation results and discussion

(1) Influence of target shape

Assume the micro-motion of the target is precession, set the angle velocity around its symmetry axis $\omega_s = 2\pi$ rad/s and the angle velocity around its precession axis $\omega_p = \pi$ rad/s respectively. The simulation results of three different shape models are shown in Fig. 6.

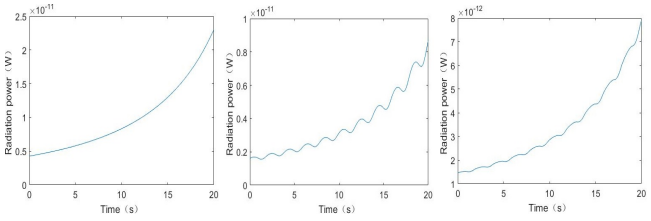


(a) Sphere (b) Cylinder (c) Cone

Fig. 6. Simulation results of different shape models

The simulation results show that the radiation power of all the targets with different shapes received by the detector is getting larger and larger, that is because the detector is moving closer to the target gradually. It is obvious that the effective area of sphere targets to the detector during rotation and precession does not change, so the time series of its radiation power is a smooth curve, as shown in Fig. 6 (a). However, the targets with other two shapes are just the opposite, as shown in Fig. 6 (b) and (c). Moreover, the radiation power of the cylinder target has a more conspicuous fluctuation than the cone target, that is because the effective area of the cylinder target to the detector changes more prominently during rotation and precession. It demonstrates that targets with different shape models have different IR radiation characteristics. Therefore, the shape can be used as an important feature for remote aerial target recognition according to the time series of radiation power of the targets.

(2) Influence of target micro-motion model

The shape of the target is set as cone, rotation and precession are considered as two different micro-motion model for two experiments respectively. In rotation experiment, the angle velocity is set as $\omega = 2\pi$ rad/s , and in precession experiment, the angle velocity is set as $\omega_s = 2\pi$ rad/s , $\omega_p = \pi$ rad/s . The simulation results are shown in Fig. 7.

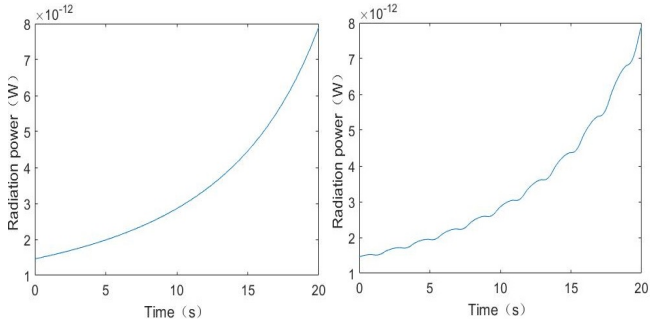


(a) Rotation (b) Precession

Fig. 7. Simulation results of different micro-motion model

The simulation results show that the radiation power of the cone target with rotation is a smooth curve, but the radiation power turns into a fluctuating curve if the micro-motion model turns into precession. That is because for an axisymmetric object, rotation around its symmetry axis does not change its attitude. It indicates that precession is the main micro-motion model that we need to analyze for the axisymmetric target.

(3) Influence of target micro-motion parameters

The shape of the target is set as cone, assume the micro-motion of the target is precession, set the angle velocity around its symmetry axis $\omega_s = 2\pi$ rad/s , and set the angle velocity around its precession axis $\omega_p = \pi$ and $\pi/2$ rad/s respectively for two experiments. The simulation results are shown in Fig. 8.

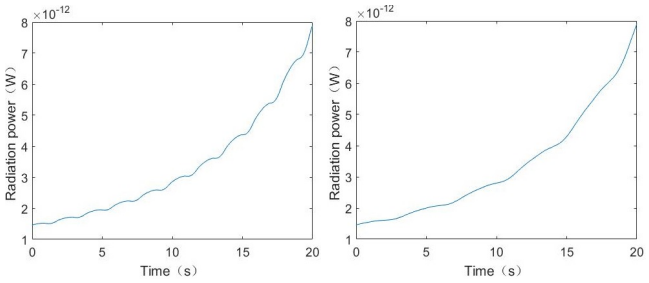


(a) $\omega_p = \pi$ (b) $\omega_p = \pi/2$

Fig. 8. Simulation results of different micro-motion parameters

The simulation results indicates that the angle velocity $\omega_p$ can be reflected in the time series of radiation power intuitively. Therefore, it can be used as a feature for remote aerial target recognition.

## IV. CONCLUSIONS

In this paper, we propose a modeling and simulation method of infrared signature of remote aerial targets, which can provide data support for the research on IR point target detection and recognition. The main highlight of this method is that it takes a comprehensive consideration of the influence of shape, material, attitude, motion and surface temperature distribution of the target. We conduct three groups of experiments to validate the method proposed in this paper. And the final simulation results demonstrate that targets with different shape or different micro-motion information have different IR radiation characteristics, which provides a feasibility of using IR signature for remote aerial targets recognition.

## REFERENCES:


[1] G. Cheng and J. Han, "A survey on object detection in optical remote sensing images," ISPRS Journal of Photogrammetry and Remote Sensing, vol. 117, pp. 11-28, 2016.

[2] W. Hou, Z. Lei, Q. Yu, and X. Liu, "Small target detection using main directional suppression high pass filter," Optik - International Journal for Light and Electron Optics, vol. 125, pp. 3017-3022, 2014.

[3] Z. Cui, J. Yang, S. Jiang, and J. Li, "An infrared small target detection algorithm based on high-speed local contrast method," Infrared Physics & Technology, vol. 76, pp. 474-481, 2016.

[4] L. Deng, H. Zhu, C. Tao, and Y. Wei, "Infrared moving point target detection based on spatial–temporal local contrast filter," Infrared Physics & Technology, vol. 76, pp. 168-173, 2016.

[5] Z. Li, Q. Hou, H. Fu, Z. Dai, L. Yang, G. Jin, and R. Li, "Infrared small moving target detection algorithm based on joint spatio-temporal sparse recovery," Infrared Physics & Technology, vol. 69, pp. 44-52, 2015.

[6] H. Qi, B. Mo, F. Liu, Y. He, and S. Liu, "Small infrared target detection utilizing Local Region Similarity Difference map," Infrared Physics & Technology, vol. 71, pp. 131-139, 2015.

[7] H. Wang and W. Zhang, "Infrared characteristics of on-orbit targets based on space-based optical observation," Optics Communications, vol. 290, pp. 69-75, 2013.

[8] H. Wang, W. Zhang and F. Wang, "Infrared imaging characteristics of space-based targets based on bidirectional reflection distribution function," Infrared Physics & Technology, vol. 55, pp. 368-375, 2012.

[9] Z. Jun, L. Rong-zhong, G. Rui, Q. He, L. Meng-meng, and O. Abdel-Hamid, "Surface Temperature Field of Projectile Flying at High Rotational Speed in Exterior Ballistic," Acta Armamentarii, vol. 34, pp. 425-430, 2013.